Springer

KSME

Journal of Mechanical Science and Technology 24 (5) (2010) 1141~1149
www.springerlink.com/content/1738-494x
DOI 10.1007/s12206-010-0320-9

Design of a hydraulic anti-lock braking system (ABS) for a motorcycle †

Chun-Kuei Huang and Ming-Chang Shih*

Department of Mechanical Engineering, National Cheng-Kung University ,Tainan, Taiwan, ROC

(Manuscript Received May 24, 2009; Revised January 14, 2010; Accepted March 4, 2010)

Abstract

This work presents a hydraulic anti-lock braking system (ABS) for a motorcycle. The ABS has a hydraulic modulator and an intelligent controller. The hydraulic modulator is analyzed, and then equipped on a scooter for road tests. The intelligent controller controls the hydraulic modulator by estimated vehicle velocity to calculate the slip ratio of the wheels in real time. The performance of the hydraulic modulator and intelligent controller are assessed by the hardware-in-the-loop (HIL) simulations and road tests. In HIL simulation, the ABS is tested for different initial braking velocities on roads with different adhesive coefficients. Furthermore, both HIL simulations and road tests are conducted on a one-phase pavement road and three-phase pavement road.

Keywords: Anti-lock brake system; Intelligent controller; Hardware-in-the loop simulation; Real road test

1. Introduction

In recent decades, many anti-lock braking systems have been developed and installed on vehicles. However, most are designed for cars or trucks, not for motorcycles. In Asia, the motorcycle is a primary mode of transportation. Therefore, an ABS for motorcycles is needed [1-6]. Generally, when motorcycles brake, those without ABSs usually trip bringing injury to riders. On wet roads in particular, riders cannot control motorcycles when the braking pressure exceeds a threshold value and the wheels lock. However, the wheels on a motorcycle equipped with an ABS would not lock during sudden braking, allowing the rider to steer the motorcycle efficiently. Moreover, an ABS on a motorcycle can reduce braking distance. However, most ABSs installed on four-wheel vehicles have hydraulic pumps and tanks. Both the size and cost of hydraulic pump and tanks limit their use on motorcycles making the ABSs installed on four-wheel vehicles unsuitable for motorcycles. This study presents an ABS for motorcycles, and tested it on a scooter.

The slip ratio is the most widely used index of the relationship between a tire and the road. Therefore, it is one of the most important issues in ABS research [7-10]. The slip ratio is derived by S=(vehicle velocity − wheel velocity)/vehicle velocity. The Pacejka research [9] showed that when the slip ratio is in the range of 8–30%, vehicle steering can be controlled because the lateral adhesive and longitudinal adhesive coefficients are high. Based on this, the slip ratio in this work is set at 20%.

In this work, the ABS is only equipped on the rear wheel of the scooter in both HIL simulations and the road tests. The front wheel is utilized to measure vehicle velocity, which is then compared with the estimated vehicle velocity calculated by the intelligent controller. Briefly, the front wheel of a motorcycle does not go on brake in the HIL simulation or the real road test. Only the rear wheel brakes using the ABS.

2. System description

Fig. 1 presents the scheme of the ABS. When a rider activates the brakes, the brake oil passes through the hydraulic modulator from the brake pump, and regulates brake oil pressure in the hydraulic modulator. The regulated brake oil is then sent to the brake calipers. When a wheel locks, the controller tells the hydraulic modulator to reduce brake oil pressure. Similarly, when brake oil pressure is insufficient, the controller tells the hydraulic modulator to increase brake oil pressure in the hydraulic modulator.

2.1 Hydraulic modulator

Fig. 2 shows the structure of the hydraulic modulator. The deactivated and activated positions of hydraulic modulator components are shown in Figs. 2(a) and 2(b). The inlet symbol shows brake oil flowing into the hydraulic modulator from the brake pump, and through the orifices to the brake calipers. The outlet symbol is the brake oil flowing into the brake cali-

† This paper was recommended for publication in revised form by Associate Editor Kyongsu Yi

*Corresponding author. Tel.: +886 6 2757575, Fax.: +886 6 2352973
E-mail address: mcshih@mail.edu.tw

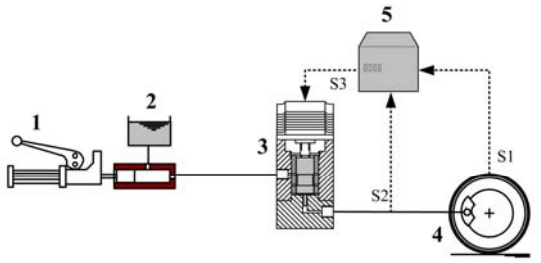

Fig. 1. Scheme of the ABS.

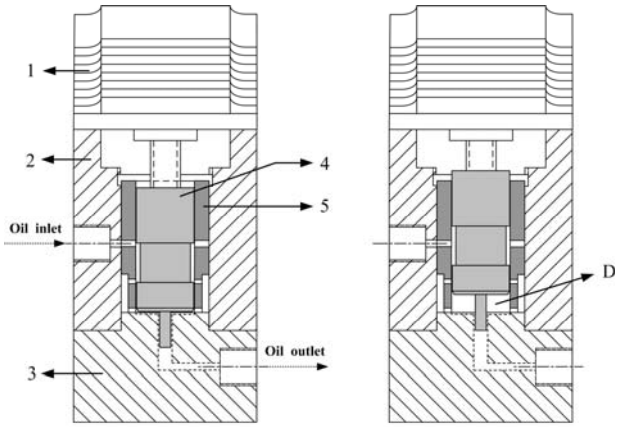

1. Motor 2. Upper case 3. Bottom case 4. Spool 5. Cylinder barrel

Fig. 2. Structure of the hydraulic modulator.

pers from the hydraulic modulator. When the hydraulic modulator is deactivated, a rider can brakes a motorcycle in the usual manner, as long as motorcycle velocity is not too fast for the ABS or oil pressure does not cause the wheel to lock.

When the ABS is deactivated, the position of the spool is as shown Fig. 2(a). If brake pressure exceeds the target value calculated by the controller, the controller sends signals to the stepping motor and the spool is raised simultaneously by the motor as shown in Fig. 2(b). At this moment, brake oil from the brake pump is separated by the hydraulic modulator. The volume of Chamber D, which is between the spool and the bottom case, is increases; thus, oil brake pressure in the brake calipers decreases. That is, the controller can reduce brake pressure by increasing the volume of chamber D or can increase brake pressure by reducing the volume of chamber D. Briefly, the controller regulates the volume of chamber D such that the brake pressure in the calipers conforms to the target pressure.

The target pressure is calculated by the intelligent controller. When motorcycle velocity is zero and the ABS is not in use, the spool in modulator returns to its initial position [Fig. 2(a)]. The cylinder barrel is made by Teflon, which can lower the friction force when the spool is moving.

Generally, when an ABS is installed on a car, the brake

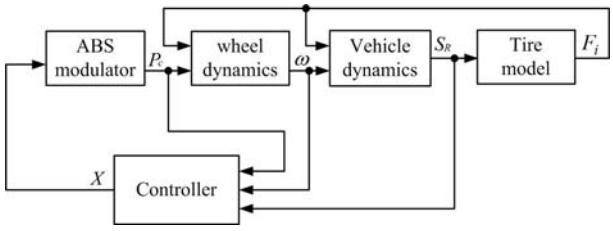

Fig. 3. Scheme of a motorcycle.

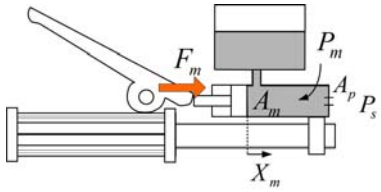

Fig. 4. Mathematical symbols of brake pump.

pedal will vibrate when the hydraulic modulator adjusts braking pressure. For motorcycles, this vibration can cause a driver to lose control of the brake handle; thus, this vibration must be prevented. The hydraulic modulator in this study obstructs the brake oil out of the orifice by the spool [Fig. 2(b)]. When the hydraulic modulator is regulated, oil pressure from the brake pump and brake calipers are isolated; therefore, a rider will not feel vibrations from the brake handle during emergency braking.

2.2 Mathematical analysis

Fig. 3 shows the relationship of the modulator, dynamics, and controller. In this section, the mathematical analyses of brake pump and ABS modulator are presented in 2.2.1 and 2.2.2. Section 2.2.3 discusses the mathematical model of vehicle dynamics and wheel dynamics. Section 2.2.4 presents the tire model. All these mathematical models were used in the simulation.

2.2.1 Brake pump

The dynamics of brake pump can be derived by

$$F_m - A_m \cdot (P_m - P_0) - C_m \cdot X_m = M_m \cdot \ddot{x}_m \tag{1}$$

$$Q_m = C_d \cdot A_p \sqrt{\frac{2}{\rho}(P_m - P_s)} \tag{2}$$

$$\dot{P}_m = \beta \frac{\dot{V}_m}{V_{mo}} = \beta \frac{Q_m}{V_{m0}} \tag{3}$$

where A_m and X_m are the cross-section area and the displacement of the piston in brake pump, C_m is the damping ratio, P_m is the brake pressure in the brake pump, V_{mo} is the initial volume of V_m, and A_p is the area of the throttle in the brake pump.

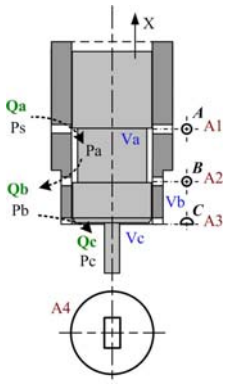

Fig. 5. Mathematical symbols of hydraulic modulator.

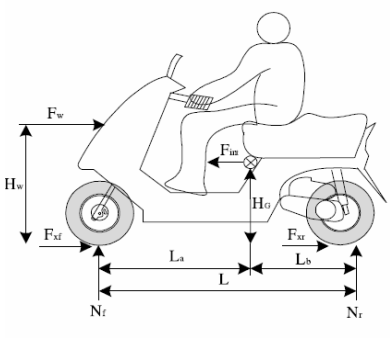

(a)

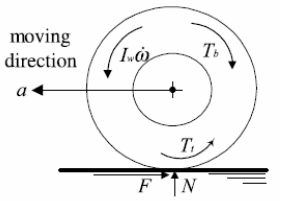

(b)

Fig. 6. Force condition on the vehicle and the wheels.

2.2.2 ABS modulator

Fig. 5 shows the mathematical symbols of the spool and cylinder barrel in the hydraulic modulator.

Oil flow rate Q_a from the brake pump to the hydraulic modulator is

$$Q_a = C_d \cdot A_1 \cdot \sqrt{\frac{2}{\rho}(P_s - P_a)} \tag{4}$$

where, P_s is the oil pressure from the brake pump, P_a is oil pressure in the volume V_a, A_1 is the cross-section area of orifice A, and ρ is the mass density.

Flow rates Q_b and Q_c are defined as

$$Q_b = C_d \cdot A_2 \cdot \sqrt{\frac{2}{\rho}(P_a - P_b)} \tag{5}$$

$$Q_c = C_d \cdot A_3 \cdot \sqrt{\frac{2}{\rho}(P_b - P_c)} \tag{6}$$

where, P_b and P_c are oil pressure in the volume V_b and the volume V_c, C_d is the discharge coefficient, and. A_2 and A_3 are the cross-section area of orifice B and C.

Therefore, the derivatives of pressure P_a, P_b and P_c are derived by

$$Q_a - Q_b = \frac{V_a}{\beta_e}\frac{dP_a}{dt} \tag{7}$$

$$Q_b - Q_c = \frac{V_b}{\beta_e}\frac{dP_b}{dt} \tag{8}$$

$$Q_c = \frac{dV_c}{dt} + \frac{V_c}{\beta_e}\frac{dP_c}{dt} \qquad V_c = V_0 + A_4 \cdot X \tag{9}$$

where, β_e is the bulk modulus, and V_b is the volume between the upper case and the cylinder barrel. The volume V_c is the total volume of chamber D and the caliper as shown in Fig. 2(b). X defines the movement of the spool, and A_4 is the cross-section area of the spool.

2.2.3 Vehicle and wheel dynamics

In this work, the motorcycle is run in a straight line without camber or steer angle. Fig. 6 shows the force condition on the vehicle and the wheels. The vehicle model can be described as follows:

$$\begin{aligned} N_f &= (M \cdot g \cdot L_b + F_{\text{int}} \cdot H_G - F_w \cdot H_w)/L \\ N_r &= (M \cdot g \cdot L_b - F_{\text{int}} \cdot H_G + F_w \cdot H_w)/L \end{aligned} \tag{10}$$

where the subscripts f and r represent the front and the rear axle, respectively; N is the normal force of each wheel; M is the total mass of the motorcycle and rider; L is the distance between the front and rear wheel. L_a and L_b are the distance from the center of gravity to the front axle and the rear axle; F_w is the longitudinal wind load equals $0.15 \cdot V_v^2$ [5], V_v is the vehicle velocity and the inertial force is defined as $F_{\text{int}} = M \cdot a = -F_w + F_f + F_r$. The damping ratio and stiffness of the suspension system and the effects of rider postures are ignored. In Fig 6(b), the wheel dynamic equation is

$$I \cdot \dot{\omega} = T_t - T_b \tag{11}$$

where I is the moment of inertia, and ω is the angular velocity. $T_b = K_b \cdot P_c$ is the brake torque, where K_b is the torque gain and P_c is oil pressure in the caliper. $T_t = F_i \cdot R$ is the torque from the tire force, where F_i is the longitudinal force and R is the radius of the wheel [5].

2.2.4 Tire model

Tire models [8-10] can be used to analyze the adhesive force between a tire and road. Many studies have attempted to develop a mathematical formula for tire, and it has two major groups. One group comprises the theoretical models based on tire construction. Another uses experimental results to define the parameters of tire models. In this work, the Pacejka 'magic formula tire model' is adopted. As the motorcycle run in a

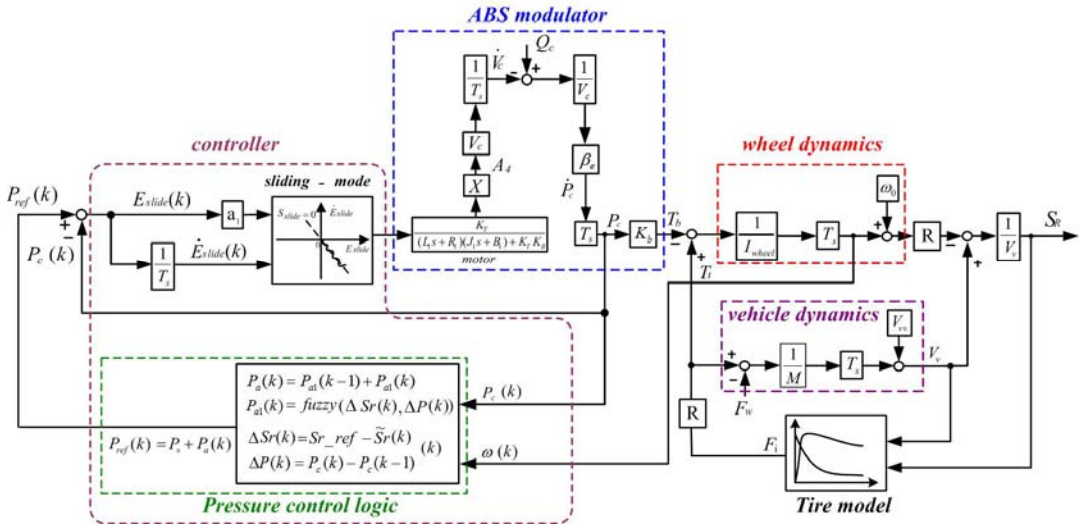

Fig. 7. Block diagram of motorcycle with the ABS.

straight line, the lateral forces from the tire are ignored. The longitudinal adhesive coefficient is defined as follows:

$$F_i = N_i \cdot \mu \quad i = f, r \tag{12}$$

$$\mu = D \cdot \sin(C \cdot \arctan\{B \cdot S_i - E[B \cdot S_i - \arctan(B \cdot S_i)]\}) \tag{13}$$

where

$$D = \mu_{\max} + C_1 \cdot V_1 \tag{14}$$

$$C = \frac{2}{\pi}\arcsin(\frac{\mu_s}{D}) + C_2 \cdot \ln(1 + C_3 \cdot V_v) \tag{15}$$

$$B = \frac{C_s}{C \cdot D} = \frac{\tan\{C_4 + C_5 / \exp[C_6 /(1 + V_v)]\}}{C \cdot D} \tag{16}$$

$$E = \frac{B \cdot S_m - \tan(\pi / 2C)}{B \cdot S_m - \tan^{-1}(B \cdot S_m)} + C_7 \cdot V_v \tag{17}$$

$$f = C_8 + C_9 \cdot V_v \tag{18}$$

S_i is the slip ratio, $\mu_{\max}$ is the maximum value of μ, and S_m is the shifted slip ratio when the peak $\mu_{\max}$ occurs. The parameters $C_1 \sim C_9$ are derived from the Pacejka model [9].

3. Controller design

Fig. 7 shows the block diagram of motorcycle, which include the proposed hydraulic modulator, controller, vehicle dynamics, wheel dynamics, and the tire model. The controller has pressure control logic and a sliding-mode controller.

The pressure control logic uses the pressure in the brake calipers $P_c(k)$ and the angular velocity of wheel $\omega(k)$ as commands, then determines the value of target brake pressure P_{ref}. Target brake pressure is defined as the standard value of pressure in brake calipers. Moreover, the sliding-mode controller causes the pressure in brake calipers to track the target brake pressure. Section 3.1 defines the pressure control logic and Section 3.2 discusses the sliding-mode controller.

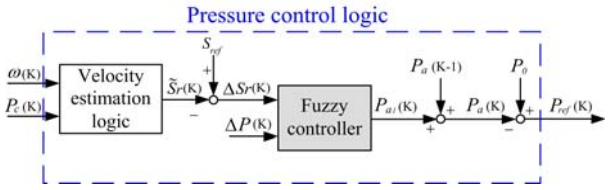

Fig. 8. Block diagram of pressure control logic.

3.1 Pressure control logic

Fig. 8 shows the block diagram of pressure control logic. The pressure control logic has a velocity-estimated logic and a fuzzy controller.

First, the velocity-estimated slip ratio $\tilde{S}_r(k)$ is determined by the velocity estimation logic, which uses the angular velocity $\omega(k)$ and the braking pressure in calipers $P_c(k)$ as its inputs, by the following equations:

$$\Delta S_r(k) = S_r\_ref - \tilde{S}_r(K) \tag{19}$$

$$\Delta P(k) = P_c(k) - P_c(k-1) \tag{20}$$

where S_r_ref is the standard value of the slip ratio defined at 0.2.

Then, $\Delta S_r(k)$ and $\Delta P(k)$ are sent to the fuzzy controller and the value of $P_{a1}(k)$ is determined. Therefore, the target brake pressure can be determined by

$$P_{ref}(k) = P_0 + P_a(k) \tag{21}$$

$$P_a(k) = P_a(k-1) + P_{a1}(k) \tag{22}$$

where P_0 is initial pressure, which can make the spool obstruct the brake oil from brake pump move fast when ABS is operating. In this study, it is set at 25 bar. The velocity estimation logic is introduced in Section 3.1.1, and the parameters of fuzzy controller are discussed in Section 3.1.2.

ΔS_r \ ΔP	NB	NS	ZE	PS	PB
NB	ZE	PS	PM	PM	PB
NS	NS	ZE	PS	PS	PM
ZE	NM	NS	ZE	PS	PM
PS	NM	NS	NS	ZE	PS
PB	NB	NM	NM	NS	ZE

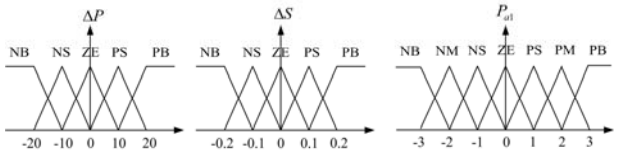

Fig. 9. Parameters of Fuzzy controller.

3.1.1 Velocity estimation logic

In the ABS controller design, slip ratio is the most important factor in determining whether a wheel is locked, because tire longitudinal force (braking force) and lateral force (handling force) are related to slip ratio. If the controller wants to adjust the slip ratio, wheel angular velocity and vehicle velocity must be measured in real time. However, vehicle velocity is not easily measured on real cars. Thus, the control rules on automobiles mostly use angular acceleration of wheels compared to threshold values, as Wu has done previously [11]. Lu [5] also presented a controller for a motorcycle, which uses vehicle acceleration for the controller command. In his experiment, vehicle acceleration was measured by an accelerometer and the controller calculated the target brake pressure. However, accelerometer measurements are easily impacted by noises of signal. Additionally, error of integral nonlinearity, or floating voltage of the zero point also influence the calculation of the vehicle velocity. Therefore, those controllers did not use the slip ratio as their command because vehicle velocity cannot be easily measured by the accelerometer on real car. In this study, the proposed velocity estimation logic calculates the slip ratio on a real motorcycle without an accelerometer.

The velocity estimation logic is applied to estimate vehicle velocity and to calculate the slip ratio in real time. From Eq. (11), the wheel dynamics are defined as $I \cdot \dot{\omega} = T_t - T_b = F_r \cdot R - K_b \cdot P_c$. According to this equation, the moment of inertia I and wheel radius R are constants, and brake torque gain K_b is considered a constant value in the different ranges of pressure value. The controller measures braking pressure P_c in the brake calipers and wheel angular velocity ω using sensors. Therefore, the longitudinal adhesive force F_r can be calculated. Similarly, the longitudinal adhesive force of another wheel F_f can be calculated using this equation. Thus, vehicle acceleration can be determined by Newton's law:

$$a = \left(F_x + F_r + F_w\right)/M \tag{23}$$

where M and F_w represent the total mass and the longitudinal wind load, respectively (Section 2.2.3). Furthermore, vehicle velocity can calculated by $V_v = V_0 + a \cdot t$, where V_0 is the initial velocity. Based on this, the estimated slip ratio can be determined.

Table 1. Parameters used for simulation.

A_1: area of orifice A in hydraulic modulator	1.57 mm^2
A_2: area of orifice B in hydraulic modulator	1.57 mm^2
A_3: area of orifice C in hydraulic modulator	6.28 mm^2
A_4: area of spool in hydraulic modulator	113.1 mm^2
R_i: radius of front and rear wheel	0.235 m
L_a: distance between front axle and center of gravity	0.86 m
L_b: distance between rear axle and center of gravity	0.58 m
L: distance between front and rear wheel	1.44 m
M: total mass of the motorcycle and rider	230 kg
λ: Sliding gain	2
k: step of sampling time	0.01 sec

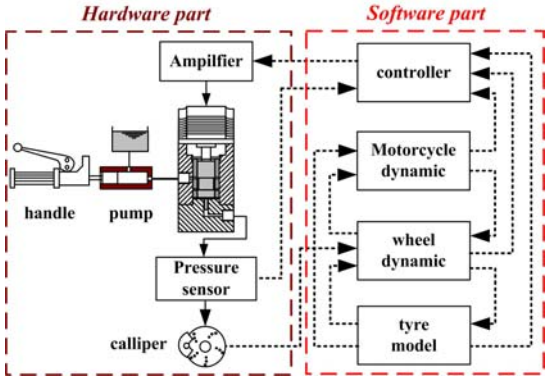

Fig. 10. Hardware and software parts in HIL simulation.

3.1.2 Fuzzy controller

Fig. 9 shows the membership functions and rule table of the fuzzy controller.

In the rule table, if the estimated slip ratio is lower than the standard slip ratio, target pressure increases. Similarly, if the estimated slip ratio is bigger than the standard slip ratio, target pressure decreases. The values of membership functions are chosen by trial and error method.

3.2 Sliding mode control

The sliding mode controller [12] makes the brake pressure in brake calipers track the target pressure. The sliding mode index is defined by the following equations:

$$S_{slide} = E_{slide} + \lambda \cdot \dot{E}_{slide} \tag{24}$$

$$E_{slide} = P_{ref} - P_c \tag{25}$$

$$\dot{E}_{slide} = \frac{dE_{slide}}{dt} = \frac{E_{slide}(k+1) - E_{slide}(k)}{period\ \ of\ \ sampling\ \ time} \tag{26}$$

where λ is a strictly positive value. All the parameters used for the simulation are shown in Table 1.

4. Hardware-in-the-loop (HIL)

Hardware-in-the-loop is a test method, in which real measurements of the physical hardware replace the mathematical model for a particular hardware during simulation [13]. Simulation via HIL is widely used in many studies, such as those on engine dynamics [14, 15] or motorcycle dynamics [16]. The purpose of using HIL simulation in this study is to simulate the motorcycle run on different adhesive coefficient roads and dangerous situations such as high speed travel of a motorcycle. Fig. 10 shows the hardware and software used in HIL simulations. The hardware comprises a brake handle, brake pump, hydraulic modulator, brake calipers, and pressure sensor. The software comprises the controller, motorcycle dynamics, wheel dynamics, and tire model.

The HIL simulation results can be divided into two sections: the one-phase pavement road test which is discussed in Section 4.1, and the three-pavement road test, which is road test on three different pavements conditions discussed in Section 4.2.

4.1 One-phase pavement road test

In this section, motorcycle braking is tested with different initial velocities on a road with a constant adhesive coefficient and constant initial velocity on two roads with different adhesive coefficients.

4.1.1 Different initial velocities road tests

Figs. 11-14 present braking results at different initial velocities of 40, 60, 80, and 100 km/hr on the road with an adhesive coefficient of 1.2 (dry asphalt road). In Fig. 11(a), the measured pressure in the brake calipers tracks the target pressure very well. Fig. 11(b) shows motorcycle velocity and rear wheel velocity with an initial braking velocity of 40 km/hr. Figure 11(c) shows the slip ratio of the rear wheel, which is kept at 0.2.

Similarly, the slip ratios for rear wheel [Figs. 12-14] are also controlled at 0.2. This means that the proposed ABS can be used when the motorcycle brakes at different initial velocities.

4.1.2 Test on roads with different adhesive coefficients

Motorcycle braking is tested on two roads with different adhesive coefficients and the same initial braking velocity (80Km/hr). The adhesive coefficients are 1.0 and 0.8 (wet asphalt road). In Figs. 15(a1) and (a2), the measured pressure in calipers efficiently tracks the target pressure. In Figs. 15(b1) and (b2), the stopping distance on adhesive coefficient 1.0 is shorter than 0.8. The slip ratios are controlled at 0.2 [Figs. 15(c1) and (c2)]. According to the test results, the ABS functioned effectively on roads with different adhesive coefficients.

4.2 Three-phase pavement road test

In this test, motorcycle braking on alternating wet and dry road (three-phase pavement road) is simulated. The

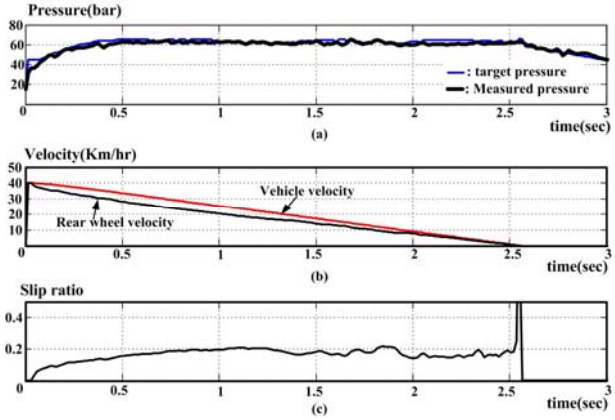

Fig. 11. HIL simulation results (initial velocity at 40Km/hr).

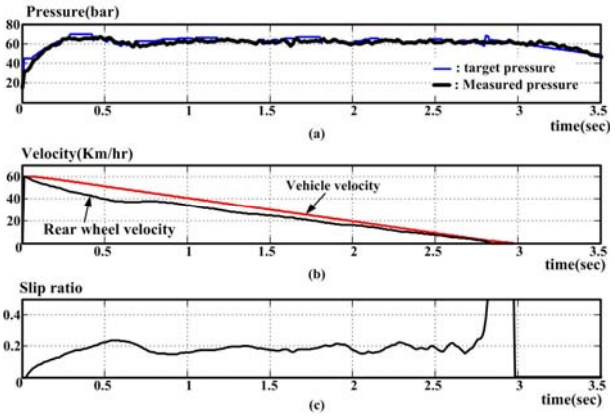

Fig. 12. HIL simulation results (initial velocity at 60Km/hr).

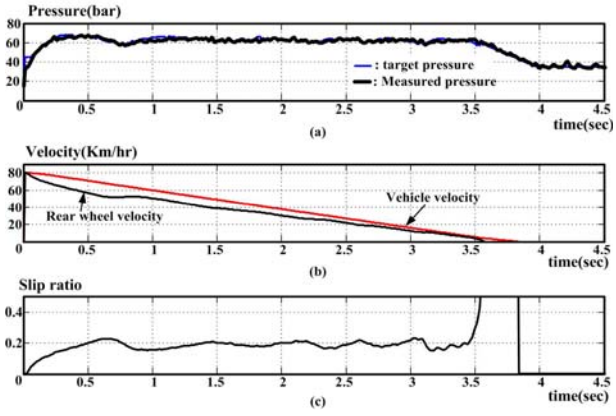

Fig. 13. HIL simulation results (initial velocity at 80Km/hr).

motorcycle brakes first on a dry road (0-0.5 sec). After 0.5 sec, the road changes to a wet road (0.5-1 sec), and then returns to a dry road. Fig. 16 shows the braking results for the initial velocity of 60 km/hr on the three-phase road.

In Fig. 16(a), target pressure decreased when the motorcycle hits the wet road to reduce the increasing slip ratio [Fig. 16(c)].

Moreover Moreover, the target pressure increased when the motorcycle hits the dry road again [Fig. 16(a)].At this moment,

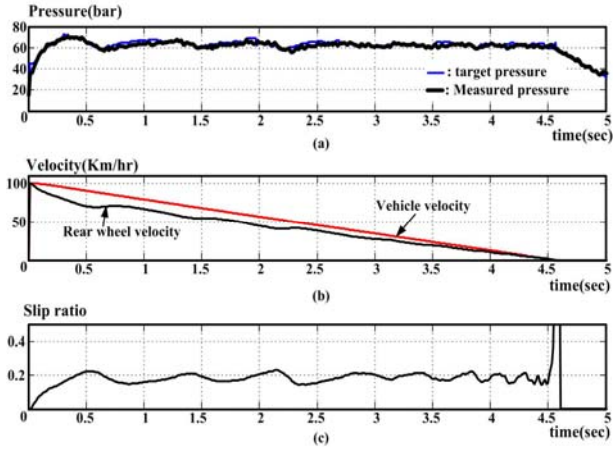

Fig. 14. HIL simulation results (initial velocity at 100Km/hr).

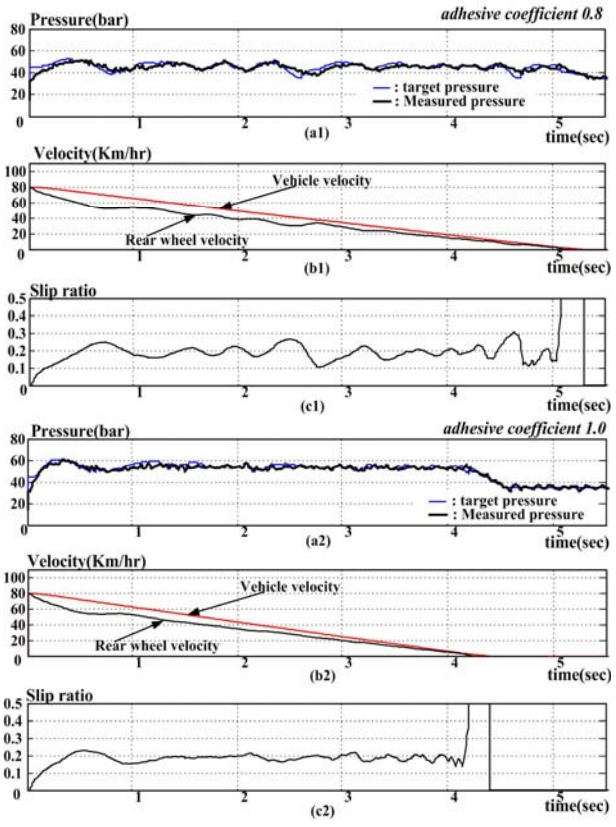

Fig. 15. HIL simulation results with different adhesive coefficient.

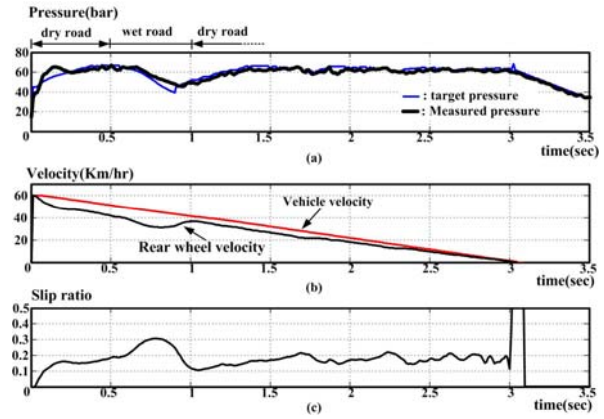

Fig. 16. HIL simulation results on three-phase road (initial velocity of 60 Km/hr).

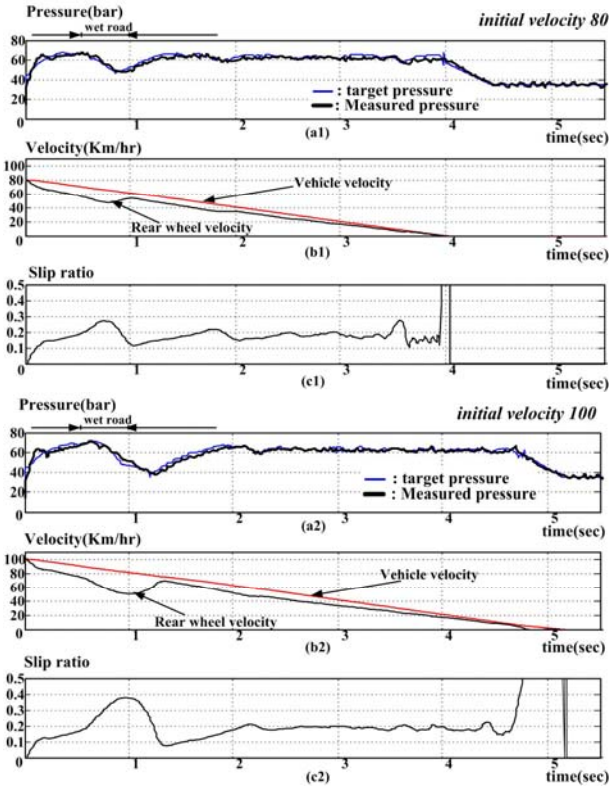

Fig. 17. HIL simulation results on three-phase pavement road with different velocities.

the slip ratio returned to the standard value of 0.2. The slip ratio is still controlled at 0.2 [Fig. 16(c)]. Motorcycle braking is also simulated at initial velocities of 80km/hr and 100km/hr on the three-phase pavement road.

Figs. 17(a1), (b1), and (c1) show braking results for an initial velocity of 80 km/hr. Figs. 17(a2), (b2), and (c2) show braking results at an initial velocity of 100 km/hr. Similarly, when the adhesive coefficient reduces, the slip ratio increases and target pressure decreases simultaneously. Conversely, when the adhesive coefficient increases, target pressure increases [Figs. 17(a1), (a2), (c1), and (c2)]. Finally, both slip ratios are kept at 0.2 [Fig. 17(c1) and (c2)]. Thus, the controller can handle the situation when the motorcycle brakes on a three-phase road at different initial velocities.

5. Real road test

After HIL simulations, the proposed ABS is installed on a real motorcycle (sym RV-180) for road testing. Fig. 18 shows photographs of the motorcycle equipped with the ABS. Fig.

Table 2. Torque gain with different brake pressure.

Brake Pressure P_c	Torque gain K_b
$P_c < 30$	8
$30 < P_c < 40$	7
$40 < P_c < 50$	6
$P_c > 50$	5

Fig. 18. Photographs of real motorcycle test.

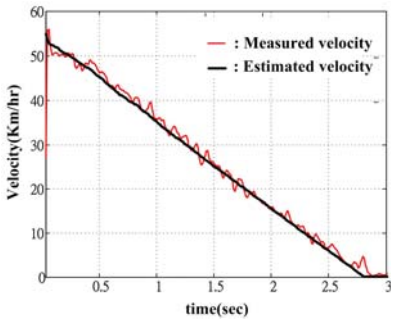

Fig. 19. Experimental result of estimated vehicle velocity.

18(a) and (b) show side view and back view of the motorcycle. Auxiliary wheels are installed on either side of the motorcycle to prevent collapse when the rear wheel locks during the test. The auxiliary wheels are installed higher than the front and rear wheels and do not touch the ground; thus, their influence can be ignored. Fig. 18(c) presents a photograph of the hydraulic modulator. Fig. 18(d) present photographs of the control box.

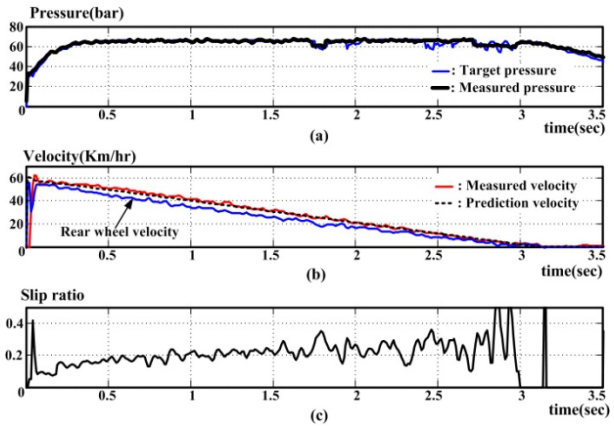

Fig. 20. Real motorcycle test results on dry asphalt.

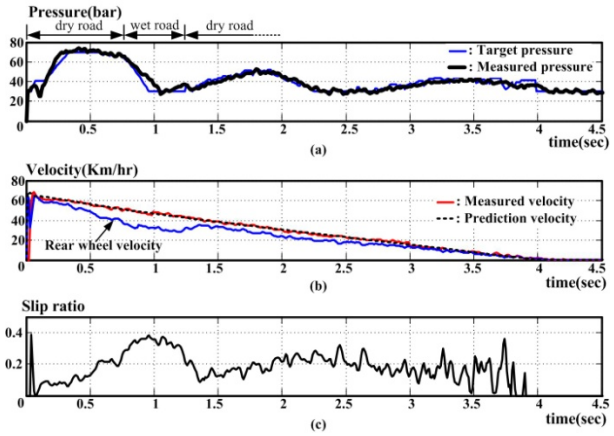

Fig. 21. Real motorcycle test results on three-phase pavement road.

Figs. 18(e) and (f) present photographs of the device used to measure front and rear wheel angular velocities. The front wheel velocity is the measured velocity in the real road test. Section 5.1 discusses experimental results of the estimated vehicle velocity. Section 5.2 shows experimental results of the real road test.

5.1 Estimated vehicle velocity test

Table 2 presents brake torque gain in Eq. (11) in the real motorcycle test, and the gain derived from the experiment result.

Fig. 19 shows the test result of estimated vehicle velocity. The bold line is the estimated vehicle velocity, which matched the measured vehicle velocity on a real motorcycle.

5.2 Real road test

Fig. 20 shows experimental results for the real motor-cycle test on dry asphalt. The brake pressure also tracks the target pressure efficiently, as in the HIL simulation [Fig. 11(a)]. The estimated vehicle velocity matches measured vehicle velocity [Fig. 20(b)]. Fig. 20(c) shows the slip ratio of rear wheel, which stays at 0.2. In addition to the test on dry asphalt, the

ABS was also tested on the three-phase pavement road. Fig. 21 shows the test results. The target pressure decreases when the motorcycle is on the wet road, and increases when the motorcycle touches the dry road [Fig. 21(a)]; the slip ratio is kept at 0.2 [Fig. 21(c)].

6. Conclusions

This work designs a hydraulic modulator, and an intelligent controller for an ABS. All of these are verified via HIL simulation and motorcycle tests. The proposed hydraulic modulator was easily fabricated. A distinct advantage is the absence of vibrations from the brake handle when the hydraulic modulator is in operation.

The HIL simulation results show that the hydraulic modulator and controller can keep the slip ratio at 0.2 with different initial braking velocities or under different adhesive coefficients. In the real motorcycle experiment, the estimated vehicle velocity is the same as the measured vehicle velocity.

According to the experimental results, the braking action of the motorcycle can safely operate on both wet and dry roads.

Acknowledgment

This research was supported by the National Science Council Taiwan, ROC (NSC97-2221-E-006-052-MY2) which is greatly appreciated by the authors.

References

[1] M. Kato, T. Matsuto, K. Tanaka, H. Ishihara, T. Hayashi and W. Hosoda, Combination of antilock brake system (ABS) and combined brake system (CBS) for motorcycles, *SAE.,* 960960 (1996) 1284-1291.

[2] A. Strichland and K. Dagg, ABS braking performance and steering input, *SAE special publications,* 980240 (1998) 57-64.

[3] F. M Georg, F. G. Gerard and C. Yann, Fuzzy Logic Continuous and Quantizing Control of An ABS Braking System, *SAE.,* 940830 (1994) 1033-1042.

[4] N. Miyasaki, M. Fukumoto, Y. Sogo and H. Tsukinoki, Antilock brake system (M-ABS) based on the friction coefficient between the wheel and the road surface, *SAE special publications,* 900207 (1990) 101-109.

[5] C. Y. Lu and M. C. Shih, Application of the Pacejka Magic Formula Tyre Model on a Study of a Hydraulic Anti-Lock Braking System for a Light Motorcycle, *Vehicle System Dynamics,* 41(6) (2004) 431-448.

[6] M. Sugai, H. Yamaguchi, M. Miyashita, T. Umeno and K. Asano, New Control Technique for Maximizing Braking Force on Antilock Braking System, *Vehicle System Dynamics,* 32 (1999) 299-312.

[7] B. Ozdalyan, Development of A Slip Control Anti-lock Braking System, *International Journal of Automotive Technology,* 9(1) (2008) 71-80.

[8] H. Dugoff, P. S. Fancher and L. Segel, An analysis of tire traction properties and their influence on vehicle dynamic performance, Proceedings of the International Automobile Safety Compendium, Brussels, Belgium, *SAE.,* 700377 (1970) 1219-1243.

[9] H. B. Pacejka, *Tire and Vehicle Dynamics*, Society of Automotive Engineers, Netherlands, (2002).

[10] R. S. Sharp and M. Bettella, Tyre shear force and moment description by normalization of parameters and the magic formula, *Vehicle system dynamics,* 39 (1) (2003) 27-56.

[11] M. C. Wu and M. C. Shih, Simulated and Experimental Study of Hydraulic Anti-Lock Braking System Control Using Sliding-Mode PWM Control, *Mechatronics,* 13 (4) (2003) 331-351.

[12] Y. K. Chin, W. C. Lin, W. C. Sidlosky, M. Rule, S. Sparschu and S. Mark, Sliding mode ABS wheel slip control, *proceedings of the American control conference, Chicago,* (1992) 1-8.

[13] S. J. Lee, Y. J. Kim and K. Park, Development of Hardware-In-the-Loop Simulation System and Validation of its Vehicle Dynamic Model for Testing Multiple ABS and TCS Modules, *7th International Symposium on Advanced Vehicle Control,* (2004) 833-838.

[14] C. F. Lin, C. Y. Tseng and T. W. Tseng, A hardware-in-the-loop dynamics simulator for motorcycle rapid controller prototyping, *Control Engineering Practice,* 14 (2006) 1467-1476.

[15] D. Bullock, B. Johnson, R. B. Wells, M. Kyte and Z. Li, Hardware-in-the-loop simulation, *Transportation Research Part C* 12 (2004) 73-89.

[16] C. W. Hong and C. C. Chen, Dynamic performance simulation of a continuously variable transmission motorcycle for fuzzy autopilot design, *ImechE.,* (1997) 477-490.

Ming-Chang Shih is currently a Distinguished University Professor of Mechanical Engineering, National Cheng-Kung University, Taiwan. He received his B.S. and M.S. from the National Cheng-Kung University in 1973 and 1977, respectively. He received his Dr.-Ing. degree from the Technische Hochschule Aachen in Germany. His current research includes Pneumatic Nano-Position Control, Energy saving in hydraulic control system, Anti-lock brake System and Active Suspension system of vehicle.

Chun-Kuei Huang is currently a Ph.D. student of Mechanical Engineering, National Cheng-Kung University, Taiwan. He received the Master's degree from Department of Mechanical and Electro-Mechanical Engineering of the Sun Yat-Sen University in 2005. His research focuses on the tire model, and the dynamic characteristics and the anti-lock brake system of motorcycle.